SMOS L1 ALGORITHMS

Antonio Gutiérrez(1), José Barbosa(1), Nuno Catarino(1), Rita Castro(1), Sofia Freitas(1),
Bruno Lucas(1), Henrique Candeias(1), José Freitas(2), Marco Ventura(2), Michele Zundo(3)

(1) Ground Segment Systems, Deimos Engenharia, S.A.; Lisboa, Portugal
(2) Command and Control, Critical Software S.A.; Lisboa, Portugal
(3) European Space Agency; Noordwijk, The Netherlands

ABSTRACT

The Level 1 Processing of SMOS transforms the data acquired by MIRAS (Microwave Imaging Radiometer with Aperture Synthesis) into geolocated TOA Brightness Temperatures, providing observation angles and additional parameters for the Level 2 Processor.

Prior to SMOS launch in November 2009 the Level 1 Prototype Processor (L1PP) lead the way for specifying product types and contents, as well as to define, implement and validate all processing algorithms.

During the six months of Commissioning, L1PP continued to be the testing environment for all new algorithms and proposed modifications to the Level 1 products. Particular emphasis should be given to L1PP's capability to produce the first image from SMOS. Within less than three hours after the data acquisition at ESAC, L1PP generated images. L1PP has also been tuned to identify unforeseen hardware problems that have been spotted only with the satellite in-orbit.

This paper is divided in 3 sections: I) a high level description of the L1 processing strategy and functional blocks of the processor (called processing units); II) important results obtained during the In-Orbit Commissioning Phase (IOCP), namely for calibration optimization, image reconstruction improvement, geolocation assessment and the impact on scientific results, in particular, to insure optimal input to Level 2 Soil Moisture and Ocean Salinity retrieval; and III) conclusions from the Commissioning Phase.

Keywords – SMOS; L1 processing; software; algorithms; commissioning

1. PROTOTYPE ARCHITECTURE AND PRODUCT TYPES

The L1PP is data driven, so processing is triggered by polling of the input directories. L1PP has been designed in such a manner that each of its three modules is independent, allowing changes in the current algorithms or the implementation of new ones without impacting the rest of the prototype's code. The interface between the three modules is done though the writing and reading of products that are defined according to standard XML schemas that are defined according to the product specification. [08]

The first module (Level 1a) is responsible for transforming raw data coming from the instrument into calibration products and using them to obtain calibrated visibilities, which are the main output of this module. The next module (Level 1b) is the core of L1PP, where L1a calibrated visibilities are transformed into brightness temperatures, after the correction of the influence of Foreign Sources. In addition, it is within this module that the G and J^+ Matrices are generated, as well as the Flat Target Transformation products. Finally, Level 1c geolocates the L1b brightness temperatures, though the use of a uniform discrete global grid over the Earth's surface. For more details please refer to [05], [06] and [02].

1.1. Level 1a Processing

The payload has 72 receivers (also called LICEFs) and each pair of them forms a baseline. There are 2556 possible baselines that measure a visibility. In order to calibrate these visibilities, it is necessary to derive calibration parameters from L0 Calibration data and to perform periodical internal calibration. There are two modes of internal calibration: a) correlated noise injection – where the same signal is fed by the noise sources to the LICEFs and the phase differences between them are calculated; and b) uncorrelated noise injection – where the LICEFs receive random signals and the residual offsets for each baseline are computed.

To show the importance of having good calibration parameters, Figure 1 presents two orbits processed at different stages of the IOCP. The browse product represented on the left side has been processed right after the Switch-On of MIRAS on mid December 2009. At that point, only On-Ground characterization of MIRAS was available and as it can be seen, L1PP was able to process and retrieve a temperature map that reflected reality – the land was at ~300 K, the sea at ~100 K. The problem was the lack of the

correction for the Fringe Washing-Function (FWF) phase, computed from correlated noise injection calibration. The browse product on the right side shows an orbit acquired during the rainy season in Australia in February 2010 and has been processed by L1PP on March 2010, using all calibration parameters derived from In-Orbit data – the blur on the coastlines caused by the lack of information on the FWF phase is gone. (For an in-depth description of MIRAS calibration and Level 1a processing, please refer to [05])
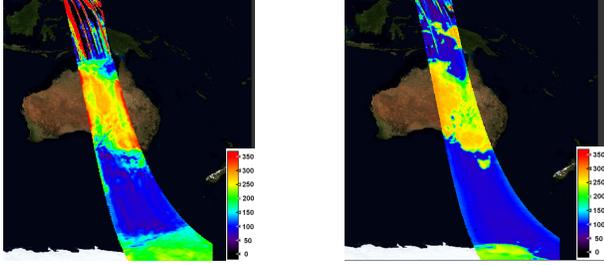

Figure 1: H-pol browse for two orbits over Australia (Left: Acquired and processed in 18-Dec-2009 with On-Ground calibration; Right – Acquired on 16-Feb-2010 and processed on March 2010 with In-Orbit calibration)

1.2. Level 1b Processing

This module transforms the L1a calibrated visibilities into Brightness temperatures. It is divided in three processing units a) Foreign Sources b) Error Mitigation and c) Image Reconstruction – where the final L1b visibilities are transformed to the Brightness Temperature Fourier components, $\hat{T}$, by the linear application of the (pseudo-)inverse System Response, J^+, to the visibilities: $\hat{T} = J^+V$.

The Foreign Sources unit removes all the unwanted contributions (Sun, Moon, Sky and Backlobes) from the image to be reconstructed. The brightness temperatures for these sources are transformed to the visibility domain, ΔV_{FS}, through the use of the System Response Function (G-matrix) and then subtracted from the L1a visibilities, V_{L1a}.

The Error Mitigation is crucial in the L1 processing chain since it is in this unit that the Flat Target Transformation (FTT) is applied and the same reference temperature is set to ΔV_{FS} and V_{L1a}. The FTT is the method devised to remove residual errors from the instrument that can not be calibrated in L1a – in particular, the Antenna Pattern Errors. (More details about the image reconstruction process can be found in [06].)

1.3. Level 1c

The last module of L1PP is responsible to geolocate the Brightness temperatures computed in the antenna frame to the Earth's surface, as well as to calculate several parameters to be annotated in the L1c product for Level 2 teams to use in their models to derive Soil Moisture and Ocean Salinity.

(For more information on geolocation routines, please refer to [02].)

2. COMMISSIONING ACTIVITIES

During the IOCP several studies were carried out using L1PP. In this section the most interesting results will be presented. Other particular studies, namely for RFI mitigation, have been performed and are presented in [01].

2.1. Instrument Performance

A special maneuver was executed during the IOCP, in order to assess on MIRAS' performance between Dual and Full Polarimetric mode. Using the only well known target to MIRAS – i.e. the flat unpolarised Sky, the instrument was kept in inertial pointing for 35 minutes where, in the first half, SMOS captured data in Dual polarimetric mode and, for the rest of the maneuver, , the instrument mode was switched to Full. The data was analyzed and this section presents the key results obtained from it. (An extensive analysis of this maneuver can be found in [09].)

2.1.1. Accuracy
The instrument accuracy is assessed thought the analysis of a Flat Target Response (FTR) processed using the Sky Removal algorithm and applying the FTT. The accuracy can be defined as

$$Acc = \sqrt{\left\langle \overline{T}\left(\xi,\eta\right)\right\rangle^2 + \tilde{\sigma}^2} \qquad \text{Eq. 1}$$

where $\left\langle \overline{T}\left(\xi,\eta\right)\right\rangle$ is the average Time Averaged Temperature in a selected domain (full Hexagon, Alias-Free Field of View (AF-FOV) or Circle of radius 0.3) and $\tilde{\sigma}$ is its Space Standard Deviation.

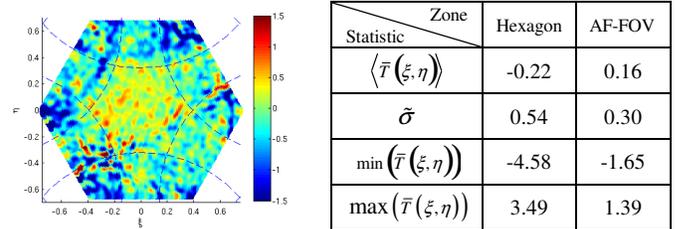| Statistic \ Zone	Hexagon	AF-FOV
$\left\langle \overline{T}\left(\xi,\eta\right)\right\rangle$	-0.22	0.16
$\tilde{\sigma}$	0.54	0.30
$\min\left(\overline{T}\left(\xi,\eta\right)\right)$	-4.58	-1.65
$\max\left(\overline{T}\left(\xi,\eta\right)\right)$	3.49	1.39

Figure 2: Time Averaged Temperature for 150 Snapshots in Dual Polarisation for the FTR for 19-Jan-2010 (H-pol)

Figure 2 shows the overall aspect of $\overline{T}\left(\xi,\eta\right)$ for the image of the Sky processed by L1PP under the conditions specified. Note that $\overline{T}\left(\xi,\eta\right)$ is centered at zero and the average value, both in the AF-FOV and the hexagon is ~0K.

Using Eq. 1, the accuracy for the two polarimetric modes and their polarisations has been computed and is presented in Table 1. Except for the hexagon, the accuracy is always lower than 0.35 K. There is an expected degradation in the accuracy of ~40% when changing from dual to full

polarimetric mode. Taking the values in the Circle r = 0.3, it is found that there is a degradation of ~6 and 4% for H- and V-pol, respectively.

Mode	Pol.	Hexagon	AF-FOV	Circle r =0..3
Dual	H	0.580	0.335	0.337
	V	0.694	0.273	0.279
Full	H	0.749	0.328	0.316
	V	0.777	0.286	0.291
	Re(HV)	0.435	0.319	0.312
	Im(HV)	0.367	0.256	0.251

Table 1: Accuracy computed by L1PP v3.3 for 19-Jan-2010 FTR

2.1.2. Radiometric Sensitivity

The Radiometric Sensitivity is defined as the minimum detectable brightness temperature signal [11]. It can be computed using

$$\bar{\sigma}(\xi,\eta) = \sqrt{\frac{1}{N}\left(\sum_{n=1}^{N} T_n(\xi,\eta)^2\right) - \bar{T}(\xi,\eta)^2} \qquad \text{Eq. 2}$$

where N is the number of snapshots with brightness temperature, $T_n(\xi,\eta)$, used to compute the Time Averaged Temperature (time average denoted by the overbar). Table 2 shows the average value of the Radiometric Sensitivity in the Circle r = 0.3. The ratio of $\bar{\sigma}(\xi,\eta)$ between Full and Dual polarization for H- and V-pol is 1.37 and 1.34, respectively. This experimental value shows some discrepancy from the one predicted theoretically, 1.41, which is computed as a ratio of the integration time of Dual H-pol scenes against Full H-pol scenes, as described in [07] and [09]. These results lead to the re-evaluation of the effective integration time of scenes acquired in Full Polarimetric mode [02] and [09].

Mode \ Pol.	H	V	Re(HV)	Im(HV)
Dual	1.535	1.527	-	-
Full	2.110	2.051	2.037	2.047

Table 2: Radiometric Sensitivity in the Circle r = 0.3 for 19-Jan-2010

Figure 3 shows the average value of the Radiometric Sensitivity computed for six FTRs acquired in Full Polarimetric mode during the IOCP. It can be seen that this statistic has a small variation, both within each polarization (worse case is $|\Delta| = 0.04$, in V-pol), as well as when comparing all polarizations (maximum variation is $|\Delta| = 0.08$) – this can be interpreted as a good indicator of the instrument stability during the six months of IOCP.
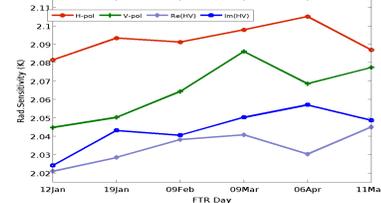

Figure 3: Average $\bar{\sigma}(\xi,\eta)$ in the Circle r = 0.3 for six FTRs

2.1.3. Dual versus Full Polarimetric modes

The FTR used to assess on the Accuracy of MIRAS has also been used to evaluate the impact of setting SMOS to operate on Full or Dual Polarimetric mode. It has been observed that, for the same target, Dual and Full Polarimetric modes produce images with slightly different statistics, but following the theoretical predictions.

When comparing the Time Averaged Temperature maps obtained with MIRAS in both Polarimetric modes, it has been verified that the images are effectively the same since a) the differences in the AF-FOV have an average of -0.16 ± 0.32 K, for the worse polarization (H-pol) and b) the resulting image is deprived of any pattern, i.e. the differences are random.

2.2. Baseline Weights Algorithm

Out of the 2346 baselines availale to be reconstructed to generate the final image, some of them are known to be erroneous (the NIR-NIR across arm baselines and the baselines across hinges), while the NIR-LICEF (or Mixed) baselines are noisier than LICEF-LICEF baselines. With this knowledge it is possible to remove and weight down the worst baselines from the image reconstruction process. This is done through the use of a weighing matrix applied both to the visibilities and to the J^+ Matrix.

Using the same methodology as in [03], the ratios between the Mixed baselines and LICEF-LICEF baselines have been computed for ~5 months of data [04]. Figure 4 shows these values for ascending and descending orbits, in H- and V-pol. The solid and dashed lines represent the average ratios, computed discarding the first two observations. As it can be seen, the ratio between Mixed and LICEF-LICEF baselines is very stable and there isn't a clear distinction between ascending and descending orbits (due to the amount of observations needed to compute the radiometric noise levels, the results presented in Figure 4 were computed using data processed by the Level 1 Operational Processor (L1OP). The initial instabilities in L1OP in terms of calibration assumed to be the cause of the strange values obtained for January and February). These ratios are then used to compute weights ($w_b = 1/R$) to be applied to the visibilities and to the J^+ Matrix.
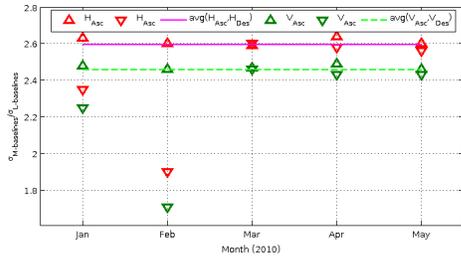
Figure 4: Temporal Evolution of the Ratio between Radiometric Noise levels between Mixed and LICEF-LICEF baselines

At Level 1, the variable that quantifies the improvements of the baseline weights algorithm is the radiometric sensitivity. In order to analyse it, the same orbit is processed twice with different weighting matrices and respective J^+ matrices. Using the results obtained by L1PP, the radiometric sensitivity is computed and shown in Figure 5.

Computing the differences between the figures presented in Figure 5 (and their analogues for V-pol) it has been found that the radiometric sensitivity is improved, in average by 0.2 K inside the Circle r = 0.3 for H- and V-pol.
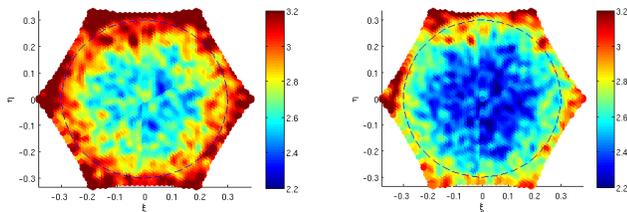

Figure 5: Radiometric Sensitivity in H-pol computed with two different weighing matrices – Left: Default Weights, Right: Sea Weights (~500 scenes acquired on the Pacific Ocean in latitudes between ± 40º on 10-Mar-2010 at 14:59, aprox.)

4. CONCLUSIONS

4.1. Summary

The Level 1 Prototype Processor was well prepared to be used in the Commissioning Phase. The existence of several flags to switch on/off the algorithms to be used was crucial during Commissioning. For example, the flag to control the decimation of the Local Oscillator phase was extensively used to assess on the final rate selected – sampling each 10 minutes [10].

L1PP was often used to assess on MIRAS' performance. In this paper results for the Radiometric Sensitivity and Accuracy were presented, and it was shown that both of these figures of merit are compliant with the requirements. [11] The requirement for the Radiometric Sensitivity was that it should be lower than 2.5 K at boresight (worse value obtained is 2.3 K, for Mixed Scenes in V-pol) and the systematic error (represented by the Accuracy) should be smaller than 1.5 K. The later is achieved with values of Accuracy below 0.5 K but these have been computed for the Sky. It is still mandatory to improve the Accuracy for measurements over the Earth.

Furthermore, the baseline weights algorithm, implemented first in L1PP, was shown to increase the Radiometric Sensitivity of the data by around 0.2 K.

An in-depth analysis of the Radiometric Sensitivity for the two instrument modes and their polarizations led to several corrections in estimates for Full Polarisation Mode – namely on theoretical and effective integration times.

4.2. Other Acheivements

Level 1a validation has been conducted along side with CASA and UPC and V_{L1a} computed with L1PP match up to 10^{-5} K with the ones computed independently by the MIRAS Testing Software (MTS). Unforeseen hardware problems (incorrect lock of the LO frequency) have been detected during the Commissioning Phase. L1PP has been equipped with the functionality to detect and cope with these problems, but an operational solution needs to be devised.

REFERENCES

[8][01] A. Camps, J. Gourrion, J. Tarongí, A. Gutierrez, J. Barbosa, R. Castro, "RFI Analysis in SMOS Imagery", IGARS 2010, July 2010

[5][02] A. Gutierrez, R. Castro, "SMOS L1 Processor L1c Data Processing Model", SO-DS-DME-L1PP-0009, Issue 2.7, 31-May-2010, SMOS Project Documentation

[1][03] E. Anterrieu, H. Carfantan, M. Martin-Neira, J. Barbosa, and R. Castro, "Estimating and accounting for the covariance matrix of the MIRAS instrument onboard SMOS", Accepted for oral presentation at the 11th Specialist Meeting on Microwave Radiometry & Remote Sensing Applications (µRAD'10), Washington (District of Columbia), 1-4 March 2010.

[2][04] E. Anterrieu, Private Communication, 14 June 2010

[9][05] J. Barbosa, A. Gutierrez, "SMOS L1 Processor L0 to L1a Data Processing Model", SO-DS-DME-L1PP-0007, Issue 2.12, 31-May-2010, SMOS Project Documentation

[10] [06] J. Freitas, J.C.Correia, N. Catarino, "SMOS L1 Processor L1a to L1b Data Processing Model", SO-DS-DME-L1PP-0008, Issue 2.12, 31-May-2010, SMOS Project Documentation

[6][07] M. Martin-Neira, "Estimation of the Average Noise Ratio in the Circle between Dual and Full Pol Modes", 10-May-2010

[7][08] M. Zapata, B. Bengoa, "SMOS Level 1 and Auxiliary Data Products Specifications", SO-TN-IDR-GS-0005, Issue 5.16, 31-May-2010, SMOS Project Documentation

[3][09] R. Castro, "SMOS L1PP MIRAS Performance for Dual and Full", SO-TN-DME-L1PP-0237, Issue 1.4, 02-Jul-2010, SMOS Project Documentation

[11][10] R. Oliva, "Local Oscillator Decimation Study", Version 6.0, 7-May-2010

[4][11] SMOS Team, "SMOS Systems Requirements Document", SO-RS-ESA-SYS-0555, Issue, 4.1, 28-Sep-2004